Detection of Early Pneumonia on Individual CT Scans with Dilated Convolutions

Iurii Krak[a,b], Olexander Barmak[c] and Pavlo Radiuk[c]

[a] *Taras Shevchenko National University of Kyiv, Kyiv, 64/13, Volodymyrska str., 01601, Ukraine*
[b] *Glushkov Cybernetics Institute, Kyiv, 40, Glushkov av., 03187, Ukraine*
[c] *Khmelnytskyi National University, Khmelnytskyi, 11, Institutes str., 29016, Ukraine*

Abstract

Over the past decades, pneumonia has been considered one of the most dangerous diseases, leading to severe consequences in a short time. Without proper and timely treatment, pneumonia can lead to fatal consequences. Thus, early diagnosis and detection of this lung disease are crucial in successful treatment and constant monitoring. Indeed, there is a high demand for the development of medical image technologies for disease identification. In this paper, we propose a novel information technology for robust feature identification and early detection of pneumonia on computer tomography scans. We also propose a new modified convolutional neural network as a core feature extractor. An effective dilated convolution operation with different rates, combining features of various receptive fields, was utilized to detect and analyze visual deviations in targeted images. Due to applying the dilated convolutions, the network avoids significant losses of objects' spatial information while providing low computational losses. The investigated model classifies computed tomography images with a validation accuracy of up to 96.12%. Overall, our approach requires much fewer computing resources, proving its effectiveness for solving practical problems on available computing devices.

Keywords

Pneumonia detection, computer tomography, feature extraction, deep learning, convolutional neural network, dilated convolution, individual approach.

1. Introduction

Over the past decades, the lower respiratory tract's infectious diseases have been considered the most common causes of death throughout the world. In particular, in 2017 [1], approximately 2.17 million people died worldwide due to airway inflammation exacerbation. Besides, the COVID-19 coronavirus pandemic has further exacerbated the lethal effects of lung diseases. Various clinical studies confirmed that people with COVID-19 infection regularly suffer from severe pneumonia [2, 3]. Meanwhile, the quantitative difference between the level of infection and mortality [4] shows the critical importance of early diagnosis of pneumonia. From the clinical studies [5], we know that pneumonia is an inflammatory disease of the lungs that primarily affects tiny air sacs known as alveoli. Its severe external symptoms are dry cough, difficulty breathing, chest pain, and fever.

To date, the most general approach to diagnosing pneumonia is a chest X-ray method called computed tomography (CT) [6, 7]. A CT image is formed on a metal surface by the passage of a concentrated beam of X-ray photons through the soft and hard tissues of the body. At diagnosis, it is necessary to compare the white spots on the image with infiltrates that identify the infection and white

---

areas with pneumonic fluid in the lungs. Fig. 1 represents examples of CT scans with different types of pneumonia.
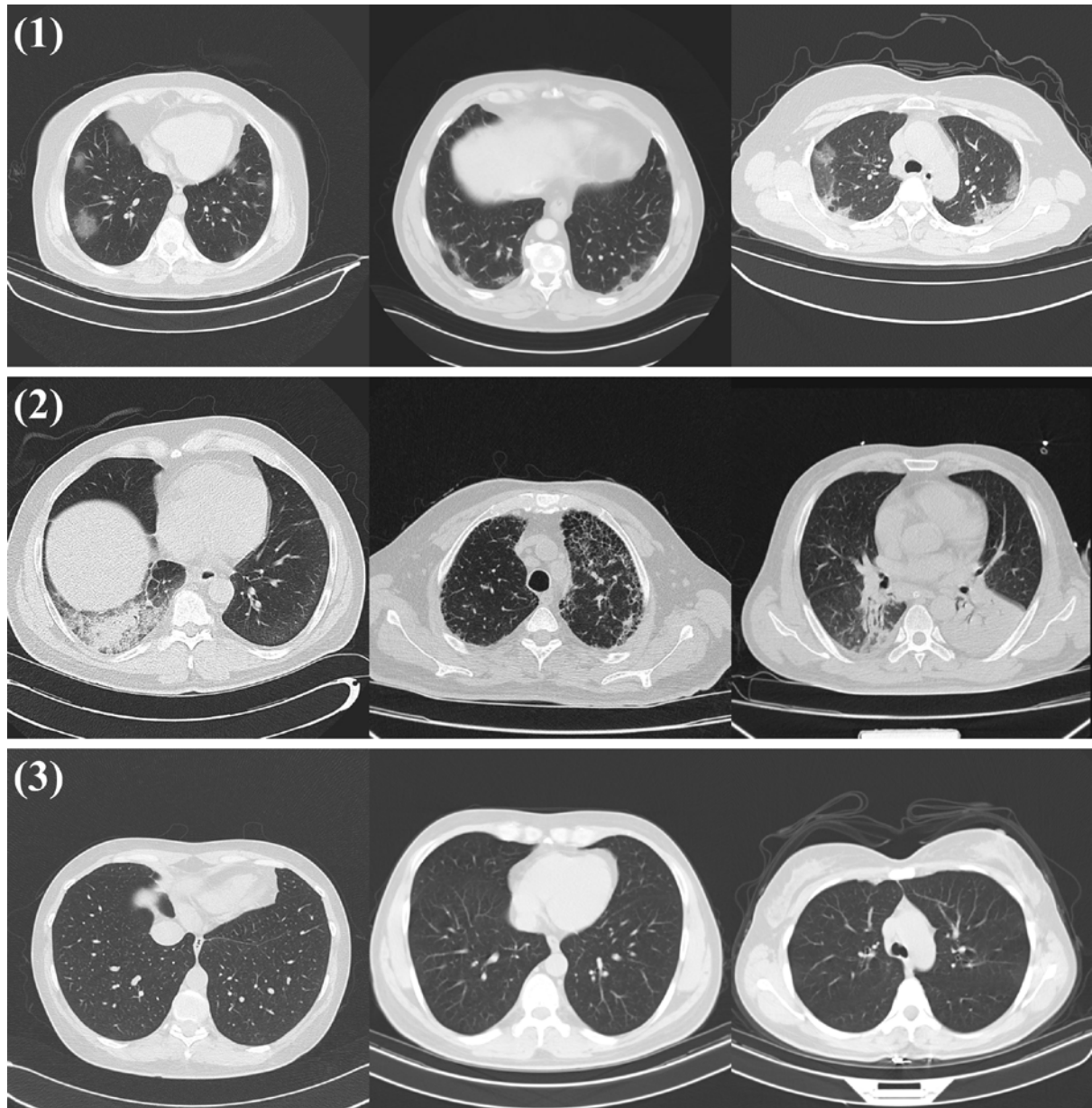
Figure 1: CT samples images extracted from the COVIDx CT-2 benchmark dataset: (1) viral pneumonia due to SARS-CoV-2 infection, (2) common pneumonia (CP), (3) normal samples [8]

For the most part, pneumonia can be detected at the initial stages of development only by comparing images taken at intervals of 1–2 days [9]. However, a significant disadvantage of radiographs, as a means of early diagnosis of viral pneumonia, is the limited range of colors, consisting of different shades of gray. Moreover, the visual transition from air-filled tissue (normal lung condition) visible in darker shades to distinctly compacted tissue requires enough fluid to shift the image's overall color scheme to lighter shades [10, 11]. Thus, preventive actions to detect viral pneumonia are complicated by the limited color scheme of radiographs and, consequently, the weak expression of pneumonia features in CT scans.

The human factor can be a critical factor in the early diagnosis of pneumonia. Radiologists must have extensive expertise to distinguish the heterogeneous color distribution of air in the lungs. Such a distribution can be vividly expressed on the radiograph in various gray shades, but it does not correspond to the pneumonic fluid. Therefore, specialists must determine whether the white spots on

the X-ray film correspond to the liquid. Following recent surveys [12, 13], both false positive and false negative diagnoses might heavily harm human health. We may assume that the use of computational methods and the implementation of automated diagnostic systems (ADS) at an early stage of pneumonia can substantially increase the chances of correct diagnosis and, consequently, lead to successful preventive measures and further treatment.

In general, ADSs serve the clinical decision-making process, considering the study of information adequacy [14] and its noise immunity [15]. They combine computer vision (CV) and artificial intelligence (AI) techniques with X-ray and CT image processing to detect image patterns. Modern digital diagnostic systems typically operate based on machine learning (ML) methods, which detect and describe specific disease features in a CT scan. These methods are optimized for specific datasets and trained to identify predetermined changes in the size of the region of interest (ROI), orientation, and position on CT scans.

In recent years, visual feature extraction technologies [16, 17] have been widely spread, primarily based on hyperplane classification approaches [18, 19] and deep learning (DL) methods[12, 20], in particular, convolutional neural networks (CNNs) [21]. CNN has been considered the most promising method of extracting and processing objects' features in the images [22] and therefore has been employed to address CV issues in medical imaging.

However, despite CNN's significant success in various short-term problems, the lack of precise interpretation of the results does not allow CNN to show its full potential in medical diagnosis. Insufficiently studied behavior of the CNN model limits its use in everyday clinical practice [23]. To date, there is still no clear understanding of early pneumonia features on a CT scan that might indicate the computational model about the presence of the disease. Accordingly, it is not clear how to design a proper CNN topology for individual pneumonia diagnosis in the early stages. Consequently, the presented research aims to cover this gap by addressing early pneumonia prevention.

2. Related works

In recent years, the scientific community has presented many works on using machine diagnosis of pneumonia on chest radiographs. For example, in [24], active contour algorithms were used to detect the entire lung zone, and then this zone was divided into 40 ROIs. As a result of applying the two-dimensional Daubechies wavelet transform and the analysis of the main components, each region's components were removed and compared with the predicted area. In this way, the authors could segment the chest image and present ROIs with possible lung disease features.

In work [25], the authors identified pneumonia in CT scans using a modified threshold value Otsu. The presented threshold value makes it possible to separate the healthy part of the lung from the manifestations of frosted glass in the image, signaling the disease's presence.

The study [26] presents an automated diagnostic system that uses the procedure of CT voxel differentiation for sequential extraction of pneumonia features in pre-prepared areas of interest. Simultaneously, the method of reference vectors was used to train and mark the pulmonary parenchyma's ROIs, guided by the characteristics of the image's texture and shape. This approach made it possible to achieve a classification accuracy of 91%, which exceeded the radiologists' results at the time.

However, despite the decent results of traditional short circuit methods in the digital diagnosis of pneumonia, they do not reveal a few essential points. First, it is necessary to specify the ROIs manually, but it is not clear how many of them are sufficient to cover all the pneumonia features. Further, it is unknown which types of textures are most meaningful for early pneumonia, given the blurring of the X-ray image's features. Besides, for new forms of pneumonia, such as those caused by COVID-19 [27, 28], it is necessary to improve the image's chest segmentation level while maintaining a high interpretation of the results. In general, traditional CV techniques require extensive image preprocessing and manual intervention to remove specific visual features before classification. Over the past few years, such issues have been primarily addressed with DL methods, mainly using CNNs.

In 2017 Wang et al. [29] presented a modified CNN, configured to localize the ROI based on a gradient for the detection and spatial localization of pneumonia. Their work demonstrated the classification accuracy of 63.3% in pneumonia detection. Wang et al. also released an extensive

collection of frontal X-rays datasets with a size of 112,120 images that significantly facilitated the digital diagnosis of lung diseases.

In [12], the gradient imaging method combined with heat maps was applied to the ROI's localization to identify pneumonia. The authors used a 121-layer tightly coupled neural network to assess the likelihood of disease and achieved an AUC of 76.8%. In another work [30], the authors focused on visualizing the process of detecting pneumonia, using class activation maps (CAMs) to interpret the results of an automated diagnostic system. The modified VGG16 achieved 93.6% classification accuracy, and the proposed imaging approach brought us closer to understanding which features of CNN are considered essential for the clinical decision. Another approach to visualizing and interpreting deep learning is fully-connected CNN, specifically, the U-Net architecture. For example, the study [31] proposes a modified U-Net architecture with convolutional kernels of $3 \times 3 \times 3$ to segmentation abdominal organs in volumetric images of computed tomography.

Over the last few years, an approach called transfer learning has become popular, which involves transferring the values of the weights of a network trained on a single dataset to a target model of a specific task. For example, the study [6] applied a transfer training method to a 36-layer CNN to effectively classify pneumonia on a small dataset and used gradient-based CAMs to interpret the automated diagnosis output. This CNN model demonstrated an impressive classification accuracy of 96.4% on a small training dataset of 5232 X-rays.

In a recent study [32], the authors proposed an automated system for diagnosing pneumonia and COVID-19 by developing a transfer training method using a few COVID-19 CT scans. The proposed multilayer CNN uses in-depth dilated convolutions to extract various targeted features in the images effectively. Moreover, discriminant gradient-based localization is integrated to separate ROIs that may signal the presence of pneumonia. At present, the in-depth convolution approach seems to be the most promising for the early diagnosis of pneumonia without expanding the neural network topology.

Thus, the presented study investigates the problem of early detection of pneumonia on CT images. The paper describes a new individual approach to medical image classification based on simple CNN structure and modified convolutions. The article also presents the evaluation results and statistical verification of the effectiveness of individual modified CNN.

3. The proposed approach

This section describes an approach to setting the fitted CNN architecture for the early detection of pneumonia.

3.1. The modification of the convolutional layer

In this part, we formulate the task of detecting pneumonia on CT scans. The following image features have been commonly employed in image processing: target color, object shape, texture, and objects' relationship in space. CT scans of a healthy person differ from images with pneumonia by various textural features. Despite the intuitive choice of feature textures to identify the image's disease, there is no clear standard for defined textures. The discussion of their definitions is far from over [32]. Unlike image features such as grayscale and color, textures are grayscale distribution relative to a particular pixel and space. Therefore, we present the texture as a constant repetition of local space in the image.

The convolution kernel is a typical example of the mechanism of feature extraction. In a convolutional layer consisting of a plurality of filters, each neuron's input is connected to the previous layer's local receiving area, which allows removing local features in the image. Due to the convolutional layer's modification, it is possible to remove the textures' local features effectively. However, the texture does not always entirely reflect the object's essential properties [33]; thereby, using only the texture features to obtain a higher level of image content might not be the right approach. As the depth of the model increases, the feature map resolution gradually decreases, and the texture highlighted by the convolution kernel may have substantial deviations.

According to clinical diagnosis [10], CT scans' pneumonia features can be either highly compacted or diffusely distributed throughout the lung plane. Therefore, there is a need to consider the disease's

features at different observation levels [7]. In [32], Yu et al. the efficiency of dilated convolutions to expand the convolution's receptive field without multiplying the number of convolution's core parameters. Fig. 2 illustrates an idea of dilated convolutions with different expansion rates.
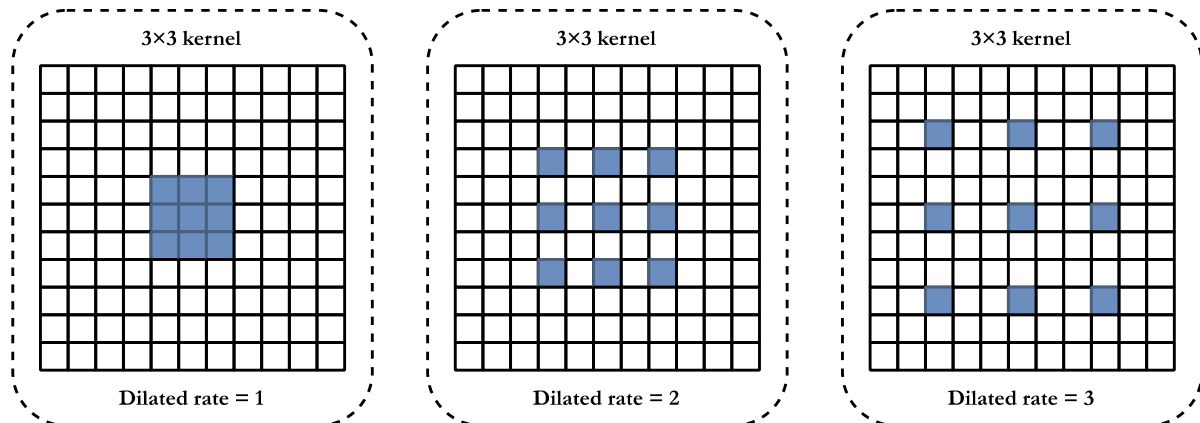
Figure 2: The scheme of dilated convolutions with a kernel size of 3 × 3. Different dilated rates cover different receptive fields with constant efficiency.

Due to the peculiarity of the expansion, various disease features, removed from different convolutions with different dilated rates, will accumulate more diversity. The traditional convolution can be divided into in-depth and dotted, one after the other. When performing deep (spatial) convolution, each input channel is individually processed by separate filters. Next, a point (traditional) convolution with 1×1 kernels is performed to integrate deep convolution results into a new space. This approach makes the extraction process computationally efficient with few convolutions [34].

In this study, we propose to apply dilated convolutions consistently with point convolutions. First, the dot convolution passes through a map of input characteristics to project information from many input channels into a more expansive space. The image is then produced through numerous deep convolutions with different spatial kernels and different dilated rates, from 1 to the maximum value of the dilation rate. We adjust the rate's value to the size of the input feature map to cover all receptive fields. As a result, in-depth convolutions extract spatial features from various receptive fields, from very condensed to generalized features. Then all the disparate features go through the next point convolution to merge into a narrow space. Such a procedure leads to removing even a few visible features of pneumonia in the image using only a few convolutional layers, which allows designing individual CNN architectures.

3.2.   The proposed architecture

This study investigates a few-layer CNN architecture based on skip connections, formerly introduced in [35]. The idea is to adjust the CNN to study minor changes removed by the rest of the convolutional layer. Thus, the network receives a set of images of 128×128 pixels after their preprocessing collapsing in a sequence of 3 convolutional layers. Convolutional filters contain 3×3 kernels with a ReLU activation function. In this way, the neurons' small size relative to the input signal's entire receptive field is provided. Accordingly, it provides an opportunity to cover the local features of the texture of pneumonia.

In general, to preserve the necessary information about the textural features of pneumonia and at the same time does not complicate the model with numerous convolutional layers, we offer a three-layer CNN with dilated convolutions. The scheme of architecture is presented in Fig. 3.
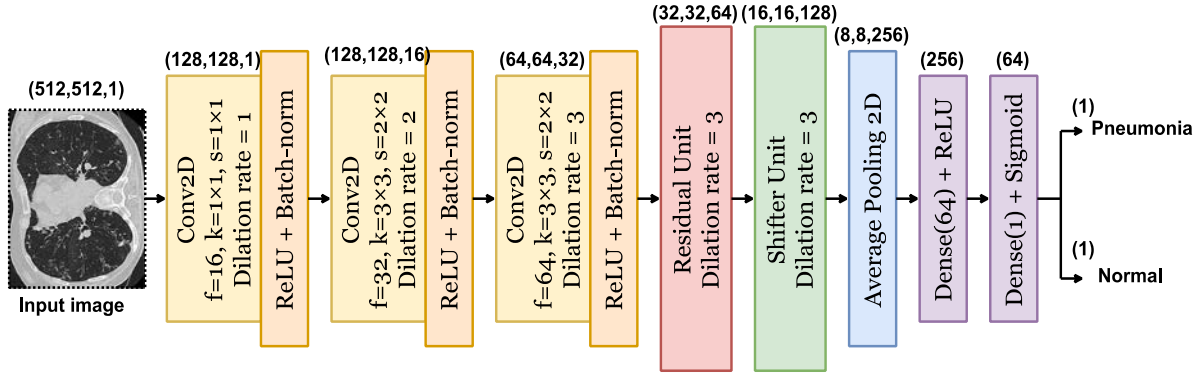
Figure 3: The proposed CNN topology designed for early diagnosis of pneumonia

This approach should ensure consistent network resolution and minimize image space resolution loss. As it is seen from Fig. 2, the dilated convolutional kernel can increase the kernel's receptive field without increasing the kernel parameters and allows avoiding excessive loss of feature map resolution. The ReLU activation function was utilized after each convolutional layer. Moreover, a normalization layer follows each convolution so that the nonlinear transformation function's input value falls into the region that is sensitive to the input data. Such an approach may avoid the problem of gradient disappearance and speeds up network learning. A dropout layer with a parameter of 0.5 has been added to prevent the model from being retrained. This layer accidentally stops the training of half of the neurons each time the training is updated and prevents hidden neurons' dependence on specific inputs. Next, we have an averaged pooling layer, which calculates each feature map's average value for the last original convolution layer. The resulting feature set is equal to the number of feature maps of the last layer and is fed to two fully connected layers. The first dense layer has 256 nodes with a ReLU activation function, the second – a classification layer with two nodes and a Sigmoid activation function to compress the two-dimensional output in the probability distribution.

4. Implementation

The proposed architecture is tested as a binary classification problem on a new publicly available dataset of CT images. The process of detecting early pneumonia using the new CNN architecture is divided into three stages: data collection, preprocessing, and image classification.

Due to the high level of stochasticity and uncertainty during neural network modeling, we investigate the effectiveness of the proposed approach against pre-configured recognized neural networks VGG19 [36], Inception_v4 [37], and MobileNet_v2 [38].

4.1. Dataset

In this study, we employed the public dataset COVIDx CT-2B [8] with chest CT images collected from 879 patients. COVIDx CT-2B contains 5,856 images with a size of 512×512 pixels, categorized into 4,273 samples of pneumonia and 1,583 samples of normal lung condition. However, to investigate early pneumonia properly, we took a subset of 3,458 CT samples with pneumonia and normal labels. The targeted subset was divided into two categories: training and validation datasets with 60% and 40% of the subset. It must be noted that the training and validation subsets comprise unique CT images, i.e., they do not intersect.

4.2. Data preprocessing and data augmentation

The next stage that introduces information technology for the early diagnosis of pneumonia is preprocessing input images. First, the visual noise level was reduced, and the image contrast was increased to improve the quality of the visual information for each input image. Moreover, we applied

intensity normalization and contrast-limited adaptive histogram alignment (CLAHE) to the targeted CT scans described in [39] to investigate our architecture.

Before performing computational experiments, the input images were normalized to the standard normal distribution to increase the contrast of the image's edges. Upon completing image processing, all images' sizes were reduced to 128×128 pixels for better bandwidth on the neural network's input layer.

The targeted pneumonia features are then extracted gradually by three convolutional layers, after which the features are smoothed to form vectorized feature maps. Next, the generated vector of features is passed to the last classification layer to attribute the image into a corresponding class. Finally, we measure the effectiveness of the proposed approach by several statistical indicators on the validation dataset.

4.3. Evaluation criteria and experiment setup

Let us consider the number of real positive (P) and real negative (N) cases in the initial data. As is known, the results of modeling and classification [16, 17, 40] are distributed as true positive (TP), true negative (TN), false positive (FP), and false negative (FN) cases. In this paper, the effectiveness of the proposed architecture together with other neural networks is evaluated by several fundamental statistical indicators defined as

$$\text{Accuracy} = \frac{TP + TN}{TP + TN + FP + FN}, \tag{1}$$

$$\text{Specificity} = \frac{TN}{TP + FP}, \tag{2}$$

$$\text{Precision} = \frac{TP}{TP + FP}, \tag{3}$$

$$\text{Recall} = \frac{TP}{TP + FN}, \tag{4}$$

$$\text{False positive rate (FPR)} = \frac{FP}{FP + TN}, \tag{5}$$

$$\text{False negative rate (FNR)} = \frac{FN}{TP + FN}, \tag{6}$$

$$F_1 = 2 \cdot \frac{\text{Precision} \cdot \text{Recall}}{\text{Precision} + \text{Recall}}. \tag{7}$$

To train the network, we used the Adam optimization method with overall 300 epochs. Based on the experiment results in [41] and the ranking of feature training in [20, 21, 42], we initialized the training parameters as follows: learning rate of $10^{-5} - 10^{-3}$, weight decay of $0.5 \cdot 10^{-3}$, momentum of 0.85, and batch size of 512.

Furthermore, following the software quality assessment guidelines from [14, 15], the computational experiments were performed using Python v3.8 and TensorFlow v.1.15 [43] as a backend. The hardware comprises an eight-core Ryzen 2700 and a single NVIDIA GeForce GTX1080 CPU with 8 GB video memory. The code is open-sourced and available via [44].

5. Experimental results

This section compares the binary classification of chest CT images based on the proposed architecture, VGG19, Inception_v4, and MobileNet_v2. Simultaneously, several experiments on the dataset were performed to test the efficiency and reliability of each of the models used. The results are presented separately through learning curves as well as accuracy and loss checks.

The learning curve is calculated based on the learning dataset. It explains how well the model learns. Simultaneously, the validation curve is calculated based on the validation dataset and explains

how well the model approximates the validation data to an ideal forecast. The loss and validation loss function is defined as the summation of the errors made for each sample of the training and validation datasets. In general, a model that approximates observational data well is less likely underfitted or overfitted. For detailed partitioning of images because of classification, the entanglement matrix for each model is also presented.

Fig. 4 presents the results of experiments conducted on the proposed architecture.
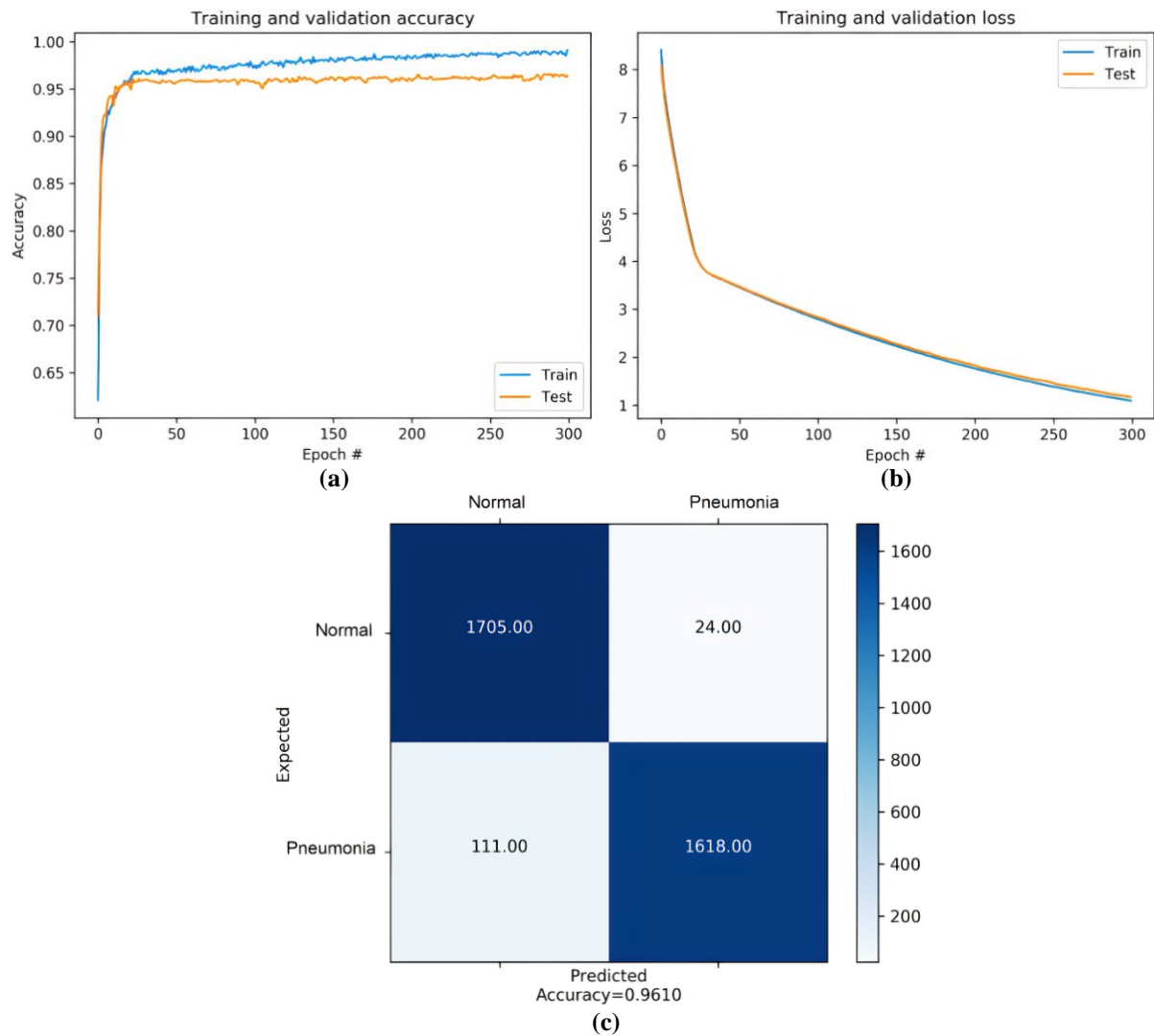
Figure 4: Accuracy (a) and loss (b) curves and confusion matrix (c) obtained by the proposed CNN

In Fig. 4a, both the training and validation curves grow to 95.51% from epoch 0 to 20. After epoch 20, training accuracy continues a slight increase and eventually reaches a value of 99.11%; meanwhile, the validation accuracy stables and stops at 96.10%.

In Fig. 4b, training and loss validation curves demonstrate excellent convergence, indicating few signs of the model's overfitting. By epoch 25, the loss function's value for both curves slows at 3.98% and then gradually falls to 1.16% in epoch 300.

Overall, the model based on our architecture could correctly identify 1,618 images as pneumonia; it incorrectly assigned 111 images with healthy lungs to the pneumonia class (Fig. 4c). Lastly, 1,705 and 24 images were marked correctly as normal and incorrectly as pneumonia for the normal class, respectively.

Fig. 5 depicts the results of experiments using the VGG19 model.

(a)

(b)

(c)
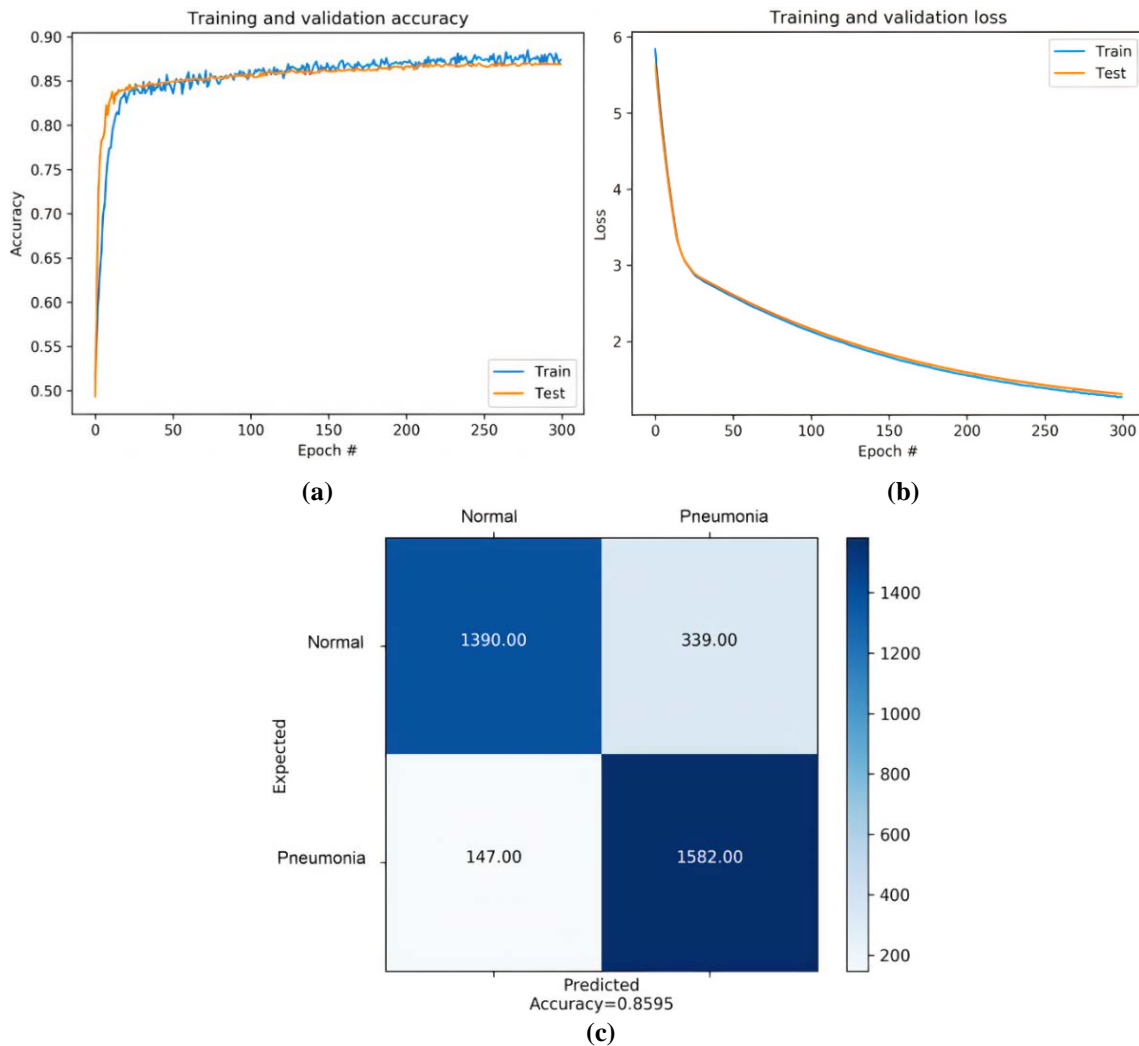
Figure 5: Accuracy (a) and loss (b) curves and confusion matrix (c) obtained by the VGG19 model

According to Fig. 5a, the training and validation accuracy curves can be divided into two intervals. There is a rapid increase in training accuracy to 84.12% and validation to 83.84% in this interval. Then the accuracy moves to the second interval, where both curves grow steadily and eventually gradually coincide to 87.37% and 86.92% in the 300 epochs, respectively. Indeed, from epoch 0 to 19, the loss functions rapidly decrease to 2.94% and then steadily decrease until epoch 300, where the training loss ends at 0.82% and validation – at 1.02% (Fig. 5b).

The VGG19 model was able to classify 1,582 images as pneumonia and 147 images as normal samples for the pneumonia class (Fig. 5c). For the normal class, 1,390 images were predicted as normal and 339 images – as pneumonia.

Fig. 6 illustrates the computational results with the Inception_v4 model.

From Fig. 6a, the training and validation accuracy curves increase rapidly to the value of 92.79% from epoch 0 to epoch 7. After epoch 7, the classification results stabilize at 97.13% and 94.59% for the training and validation datasets, respectively. A similar convergence curve is shown by the loss function curves, which sharply decrease from epoch 0 to 32 to 3.76% (Fig. 6b). Then both loss curves fall evenly to 1.62% at the last epoch.

We may observe in Fig. 6c that Inception_v4 correctly identified 1,650 samples for the pneumonia class, while 79 normal images were incorrectly marked as pneumonia. Finally, for the normal class, 1,621 and 108 images were highlighted as normal pneumonia, respectively.

(a)

(b)

(c)
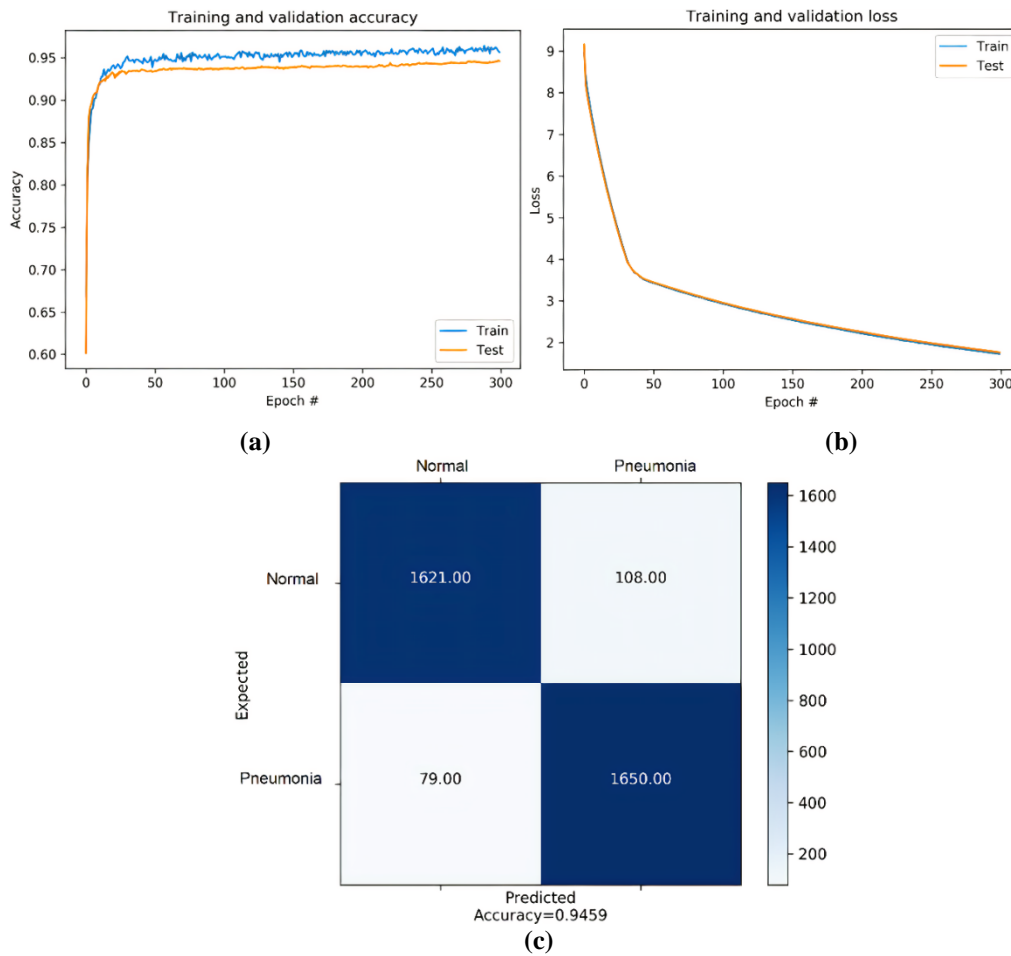
Figure 6: Accuracy (a) and loss (b) curves and confusion matrix (c) obtained by Inception_v4

Fig. 7-8 show the results of computational experiments obtained by the MobileNet_v2 model.

(a)   **(b)**
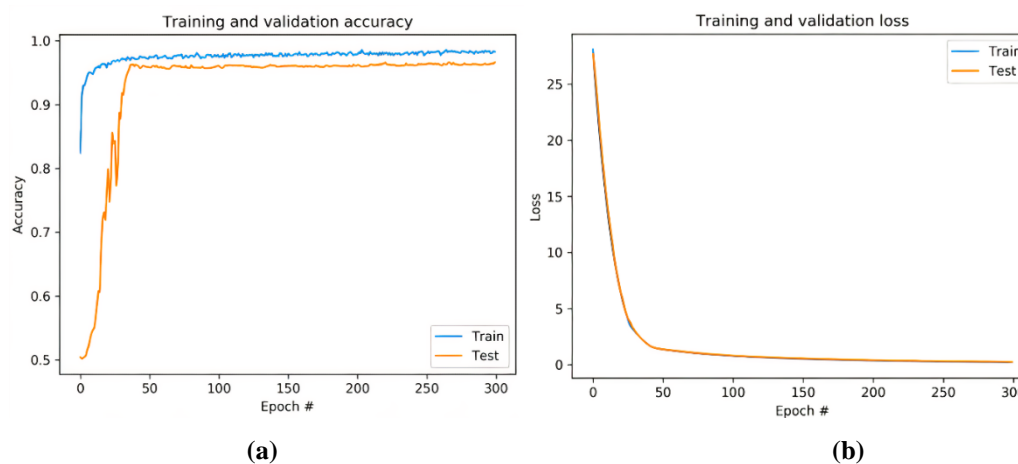
Figure 7: Accuracy (a) and loss (b) curves of the MobileNet_v2 model

As it is seen in Fig. 7a, from epoch 0 to 16, the training accuracy curve starts from 82.14% and increases sharply to 96.23%. Simultaneously, the validation accuracy sets off from 50.46% and rapidly increases to 95.91% in 42 epochs. Then, both curves gradually reach 98.17% and 96.30% in the 300 epochs, respectively. Noteworthy is the low convergence of the two curves throughout the training, which may indicate the MobileNet_v2 model's high overfitting on the COVIDx CT-2B CT image dataset. Nevertheless, MobileNet_v2 demonstrated an excellent convergence on the training

and validation losses (Fig. 7b). By epoch 44, both loss curves rapidly declined to 2.31%, slowly coinciding to 1.13% at epoch 300.

(c)
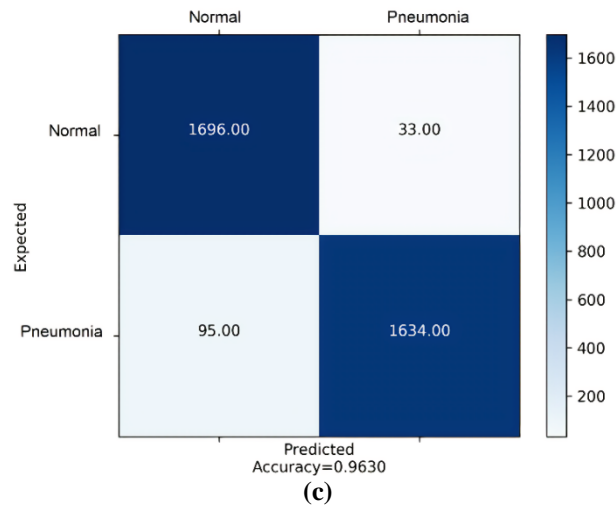
Figure 8: Confusion matrix obtained by MobileNet_v2

According to Fig. 8, the model correctly predicted 1,696 images but erred in 33 images for the normal class. Simultaneously, 1,634 images were marked correctly as pneumonia, and 95 images were identified incorrectly as normal for the pneumonia class.

6. Discussion

The presented work aims to study the identification of early-stage pneumonia on CT scans. Overall, the evaluation of the four models' effectiveness was performed according to statistical indicators (1)-(7). Tables 1-2 contain the values of the indicators obtained by the models of deep learning VGG19, Inception_v4, MobileNet_v2, and the proposed architecture for visual comparison.

Table 1
The formal results obtained by the computational experiments, %

Architecture	TP	TN	FN	FP
VGG19 [36]	1,390	1,582	147	339
Inception_v4 [37]	1,621	1,650	79	108
MobileNet_v2 [38]	1,696	1,634	95	33
The proposed architecture	1,705	1,618	111	24

Table 2
A numerical comparison of the proposed architecture with state-of-the-art models, %

Architecture	Accuracy	Specificity	Precision	Recall	FPR	FNR	F_1 score
VGG19	85.95	82.35	80.39	90.44	17.65	9.56	85.12
Inception_v4	94.59	93.86	93.75	95.35	6.14	4.65	94.55
MobileNet_v2	96.30	98.02	98.09	94.70	1.98	5.30	96.36
The proposed architecture	96.12	98.56	98.61	93.89	1.44	6.11	96.19

As we see from Fig. 5-8 and Table 1, the learning and validation accuracy curves gradually increase to the point of stability and reach a maximum of 300 epochs. It should be noted that the VGG19 model shows notably worse performance compared to the Inception_v4, MobileNet_v2

models, and the proposed architecture. Simultaneously, their training and validation curves stable starting from epoch 20, and validation accuracy stops at 94.59% for Inception_v4, 96.30% for MobileNet_v2, and 96.12% for our architecture.

Likewise, it is noteworthy that the VGG19 model shows good convergence of the learning and validation curves, which may indicate a low level of retraining of the model, and, consequently, good practical applicability of such a model. Simultaneously, other targeted models may demonstrate high validation accuracy due to retraining due to the small set of images. Experiments on a dataset with more CT images may explain the high accuracy of validation with low convergence of the learning and validation curves. Moreover, our approach showed shallow type I and type II errors, with 1.44% and 6.11%, respectively. Therefore, according to all statistical indicators (Table 2), the model based on our CNN architecture, which is schematically depicted in Fig. 3, shows satisfactory performance efficiency and can be used for further investigation.

7. Conclusion

This paper describes the application of deep learning methods for the diagnosis of early pneumonia on medical images. The proposed approach is based on CT scans classification with mild early pneumonia features using a modified convolutional neural network. The network consists of three convolutional layers with ReLU activation functions after each layer, followed by an averaged pooling layer and two dense layers. An effective dilated convolution operation with different dilated rates, combining features of various receptive fields, is utilized to detect visual deviations on the images. This approach avoids losing spatial information about the targeted objects due to dilated convolution operation while providing low computational losses due to the network's shallow depth. Computational experiments on a set of CT images and statistical comparisons with recognized neural networks in the field of computer vision have proven the computational efficiency of our architecture. Overall, the proposed CNN architecture can be an effective tool for instant diagnosis in case of the first suspicion of early pneumonia.

Further research will be aimed at optimizing the proposed approach to improve statistical metrics. It is also planned to apply additional optimization methods to tune the network's hyperparameters.

8. References

[1] G. A. Roth et al.: Global, regional, and national age-sex-specific mortality for 282 causes of death in 195 countries and territories, 1980-2017: A systematic analysis for the Global Burden of Disease Study 2017. Lancet. 392, 1736–1788 (2018). doi:10.1016/S0140-6736(18)32203-7

[2] C. Dye, R. C. H. Cheng, J. S. Dagpunar, B. G. Williams: The scale and dynamics of COVID-19 epidemics across Europe: COVID-19 epidemics across Europe. R. Soc. Open Sci. 7, 201726 (2020). doi:10.1098/rsos.201726

[3] S. J. Halpin et al.: Postdischarge symptoms and rehabilitation needs in survivors of COVID-19 infection: A cross-sectional evaluation. J. Med. Virol. 93, 1013–1022 (2021). doi:10.1002/jmv.26368

[4] B. E. Jones et al.: Computerized mortality prediction for community-acquired pneumonia at 117 VA medical centers. Ann. Am. Thorac. Soc. AnnalsATS.202011-1372OC (2021). doi:10.1513/AnnalsATS.202011-1372OC

[5] W. S. Lim: Pneumonia–overview. In: Reference Module in Biomedical Sciences. pp. 1–12. Elsevier Inc., Nottingham University Hospitals NHS Trust and University of Nottingham, Nottingham, United Kingdom (2020). doi:10.1016/B978-0-12-801238-3.11636-8

[6] J. Shen et al.: Artificial intelligence versus clinicians in disease diagnosis: Systematic review. JMIR Med Inf. 7(3), e10010 (2019). doi:10.2196/10010

[7] R. Zebari et al.: A comprehensive review of dimensionality reduction techniques for feature selection and feature extraction. J. Appl. Sci. Technol. Trends. 1, 56–70 (2020). doi:10.38094/jastt1224

[8] H. Gunraj et al.: COVID-Net CT-2: Enhanced deep neural networks for detection of COVID-19 from chest CT images through bigger, more diverse learning. Preprint: arXiv:2101.07433 (2021).

[9] C. Shen et al.: Comparative analysis of early-stage clinical features between COVID-19 and Influenza A H1N1 virus pneumonia. Front. Public Heal. 8, 206 (2020). doi:10.3389/fpubh.2020.00206

[10] A. R. Modi, C. S. Kovacs: Hospital-acquired and ventilator-associated pneumonia: Diagnosis, management, and prevention. Cleve. Clin. J. Med. 87, 633 LP – 639 (2020). doi:10.3949/ccjm.87a.19117

[11] L. Faes et al.: Automated deep learning design for medical image classification by healthcare professionals with no coding experience: a feasibility study. Lancet Digit. Heal. 1, e232–e242 (2019). doi:10.1016/S2589-7500(19)30108-6

[12] P. Rajpurkar et al.: Deep learning for chest radiograph diagnosis: A retrospective comparison of the CheXNeXt algorithm to practicing radiologists. PLOS Med. 15, e1002686 (2018). doi.org/10.1371/journal.pmed.1002686

[13] S. Waite et al.: A review of perceptual expertise in radiology-How it develops, how we can test it, and why humans still matter in the era of artificial intelligence. Acad. Radiol. 27, 26–38 (2020). doi:10.1016/j.acra.2019.08.018

[14] T. Hovorushchenko: Methodology of evaluating the sufficiency of information for software quality assessment according to ISO 25010. J. Inf. Organ. Sci. 42, 63–85 (2018). doi:10.31341/jios.42.1.4

[15] S. Lysenko et al.: Self-adaptive system for the corporate area network resilience in the presence of botnet cyberattacks. In: Gaj, P., Sawicki, M., Suchacka, G., and Kwiecień, A. (eds.) Computer Networks. pp. 385–401. Springer International Publishing, Cham (2018). doi:10.1007/978-3-319-92459-5_31

[16] Iu. G. Krivonos et al.: Human hand motion parametrization for dactilemes modeling. J. Autom. Inf. Sci. 43, 1–11 (2011). doi:10.1615/JAutomatInfScien.v43.i12.10

[17] Yu. V. Krak, A. V. Barmak, E. M. Baraban: Usage of NURBS-approximation for construction of spatial model of human face. J. Autom. Inf. Sci. 43(2), 71–81 (2011). doi:10.1615/JAutomatInfScien.v43.i2.70

[18] Iu. G. Kryvonos et al.: Predictive text typing system for the Ukrainian language. Cybern. Syst. Anal. 53, 495–502 (2017). doi:10.1007/s10559-017-9951-5

[19] A. V. Barmak et al.: Information technology of separating hyperplanes synthesis for linear classifiers. J. Autom. Inf. Sci. 51(5), 54–64 (2019). doi:10.1615/JAutomatInfScien.v51.i5.50

[20] E. Montagnon et al..: Deep learning workflow in radiology: A primer. Insights Imaging. 11, 22 (2020). doi:10.1186/s13244-019-0832-5

[21] J. A. Dunnmon et al.: Assessment of convolutional neural networks for automated classification of chest radiographs. Radiology. 290, 537–544 (2019). doi:10.1148/radiol.2018181422

[22] H. Yasar, M. Ceylan: A novel comparative study for detection of Covid-19 on CT lung images using texture analysis, machine learning, and deep learning methods. Multimed. Tools Appl. 80, 5423–5447 (2021). doi:10.1007/s11042-020-09894-3

[23] I. Domingues et al.: Using deep learning techniques in medical imaging: A systematic review of applications on CT and PET. Artif. Intell. Rev. 53, 4093–4160 (2020). doi:10.1007/s10462-019-09788-3

[24] T. Plankis et al.: Computer-aided detection of interstitial lung diseases: A texture approach. Nonlinear Anal. Model. Control. 22, 404–411 (2017). doi:10.15388/NA.2017.3.8

[25] A. Sharma, D. Raju, S. Ranjan: Detection of pneumonia clouds in chest X-ray using image processing approach. In: 2017 Nirma University International Conference on Engineering (NUiCONE). pp. 1–4 (2017). doi:10.1109/NUICONE.2017.8325607

[26] S. Jun et al.: Development of a computer-aided differential diagnosis system to distinguish between usual interstitial pneumonia and non-specific interstitial pneumonia using texture- and shape-based hierarchical classifiers on HRCT images. J. Digit. Imaging. 31, 235–244 (2018). doi:10.1007/s10278-017-0018-y

[27] Z. Feng et al.: Early prediction of disease progression in COVID-19 pneumonia patients with chest CT and clinical characteristics. Nat. Commun. 11, 4968 (2020). doi:10.1038/s41467-020-18786-x

[28] S. Tian et al.: Pulmonary pathology of early-phase 2019 novel coronavirus (COVID-19) pneumonia in two patients with lung cancer. J. Thorac. Oncol. 15, 700–704 (2020). doi:10.1016/j.jtho.2020.02.010

[29] X. Wang et al.: ChestX-Ray8: Hospital-scale chest X-Ray database and benchmarks on weakly-supervised classification and localization of common thorax diseases. In: Proceedings of the 30th IEEE Conference on Computer Vision and Pattern Recognition, CVPR-2017. pp. 3462–3471. IEEE Inc., Honolulu, HI, USA, 21-26 July 2017 (2017). doi:10.1109/CVPR.2017.369

[30] S. Rajaraman et al.: Visualization and interpretation of convolutional neural network predictions in detecting pneumonia in pediatric chest radiographs. Appl. Sci. 8, 1715 (2018). doi:10.3390/app8101715

[31] P. Radiuk: Applying 3D U-Net architecture to the task of multi-organ segmentation in computed tomography. Appl. Comput. Syst. 25, 43–50 (2020). doi:10.2478/acss-2020-0005

[32] F. Yu, V. Koltun, T. Funkhouser: Dilated residual networks. In: 2017 IEEE Conference on Computer Vision and Pattern Recognition (CVPR). pp. 636–644 (2017). doi:10.1109/CVPR.2017.75

[33] X. Feng et al.: Discriminative localization in CNNs for weakly-supervised segmentation of pulmonary nodules. In: Descoteaux, M., Maier-Hein, L., Franz, A., Jannin, P., Collins, D.L., and Duchesne, S. (eds.) Medical Image Computing and Computer Assisted Intervention − MICCAI 2017. pp. 568–576. Springer International Publishing, Cham (2017). doi:10.1007/978-3-319-66179-7_65

[34] T. Mahmud, M. A. Rahman, S. A. Fattah: CovXNet: A multi-dilation convolutional neural network for automatic COVID-19 and other pneumonia detection from chest X-ray images with transferable multi-receptive feature optimization. Comput. Biol. Med. 122, 103869 (2020). doi:10.1016/j.compbiomed.2020.103869

[35] Iu. Krak, O. Barmak, P. Radiuk: Information technology for early diagnosis of pneumonia on individual radiographs. In: Shakhovska, N., Campos, J., Melnykova, N., and Izonin, I. (eds.) Proceedings of the 3rd International Conference on Informatics & Data-Driven Medicine (IDDM-2020). pp. 11–21. CEUR Workshop Proceedings, Växjö, Sweden, 19-21 November, 2020. (2020)

[36] K. Simonyan, A. Zisserman: Very deep convolutional networks for large-scale image recognition. Paper presented at the 3rd International Conference on Learning Representations (ICLR-2015), San Diego, CA, USA, 7-9 May 2015

[37] C. Szegedy et al.: Inception-v4, Inception-ResNet, and the impact of residual connections on learning. In: Proceedings of the 31st AAAI Conference on Artificial Intelligence (AAAI-2017), San Francisco, California, USA, 4-10 February 2017. pp. 4278–4284. AAAI Press (2017). doi:10.5555/3298023.3298188

[38] M. Sandler et al.: MobileNetV2: Inverted residuals and linear bottlenecks. In: Proceedings of the 2018 IEEE/CVF Conference on Computer Vision and Pattern Recognition (CVPR-2020). pp. 4510–4520. IEEE Inc., Salt Lake City, UT, USA, 18-23 June 2018 (2018). doi:10.1109/CVPR.2018.00474

[39] R. M. James, A. Sunyoto: Detection of CT - Scan lungs COVID-19 image using convolutional neural network and CLAHE. In: Proceedings of the 3rd International Conference on Information and Communications Technology (ICOIACT-2020). pp. 302–307. IEEE Inc., Yogyakarta, Indonesia, 24-25 November 2020 (2020). doi:10.1109/ICOIACT50329.2020.9332069

[40] Iu. V. Krak, O. V. Barmak, S. O. Romanyshyn: The method of generalized grammar structures for text to gestures computer-aided translation. Cybern. Syst. Anal. 50(1), 116–123 (2014). doi:10.1007/s10559-014-9598-4

[41] P. Radiuk: An approach to accelerate the training of convolutional neural networks by tuning the hyperparameters of learning. Comput. Syst. Inf. Technol. 2, 31–36 (2020). doi:10.31891/CSIT-2020-2-5

[42] Iu. V. Krak, G. I. Kudin, A. I. Kulyas: Multidimensional scaling by means of pseudoinverse operations. Cybern. Syst. Anal. 55, 22–29 (2019). doi:10.1007/s10559-019-00108-9

[43] M. Abadi et al.: TensorFlow: A system for large-scale machine learning. In: Proceedings of 12th USENIX Symposium on Operating Systems Design and Implementation (OSDI-2016). pp. 265–283, Savannah, GA, USA, 2-4 November 2016. USENIX Association (2016).

[44] An approach to early diagnosis of pneumonia on individual computer tomography images based on the CNN information technology. GitHub, Inc., URL: https://github.com/soolstafir/Early-Pneumonia-on-Individual-CT-Scans (2021). Accessed 11 Mar 2021.